

# Hadron multiplicities and chemical freeze-out conditions in proton-proton and nucleus-nucleus collisions

V. Vovchenko,<sup>1,2</sup> V. V. Begun,<sup>3</sup> and M. I. Gorenstein<sup>4,1</sup>

<sup>1</sup> *Frankfurt Institute for Advanced Studies,*

*Johann Wolfgang Goethe University, D-60438 Frankfurt, Germany*

<sup>2</sup> *Taras Shevchenko National University of Kiev, 03022 Kiev, Ukraine*

<sup>3</sup> *Institute of Physics, Jan Kochanowski University, PL-25406 Kielce, Poland*

<sup>4</sup> *Bogolyubov Institute for Theoretical Physics, 03680 Kiev, Ukraine*

## Abstract

New results of the NA61/SHINE Collaboration at the CERN SPS on mean hadron multiplicities in proton-proton (p+p) interactions are analyzed within the transport models and the hadron resonance gas (HRG) statistical model. The chemical freeze-out parameters in p+p interactions and central Pb+Pb (or Au+Au) collisions are found and compared with each other in the range of the center of mass energy of the nucleon pair  $\sqrt{s_{NN}} = 3.2 - 17.3$  GeV. The canonical ensemble formulation of the HRG model is used to describe mean hadron multiplicities in p+p interactions and the grand canonical ensemble in central Pb+Pb and Au+Au collisions. The chemical freeze-out temperatures in p+p interactions are found to be larger than the corresponding temperatures in central nucleus-nucleus collisions.

PACS numbers: 25.75.-q, 25.75.Dw, 24.10.Pa

Keywords: proton-proton interactions, canonical ensemble, freeze-out temperature

## I. INTRODUCTION

Studies of properties of the strongly-interacting matter at extreme energies and densities is one of the main goals for high-energy nucleus-nucleus (A+A) collision experiments. The data of the NA49 Collaboration on hadron production in central Pb+Pb collisions [1–3] at beam energies  $E_{\text{lab}} = 20A, 30A, 40A, 80A,$  and  $158A$  GeV (which corresponds to  $\sqrt{s_{NN}} = 6.3, 7.6, 8.8, 12.3, 17.3$  GeV for the center of mass energy of the nucleon pair) show rapid changes of several hadron production properties. Particularly, the sharp maximum of the  $K^+/\pi^+$  ratio (the *horn*) at  $30A$  GeV predicted in Ref. [4] was found with approximate constant value of this ratio at collision energies higher than  $80A$  GeV. These data were obtained at the Super Proton Synchrotron (SPS) of the European Organization for Nuclear Research (CERN), and they have been confirmed by the Beam Energy Scan (BES) program [5] at the Relativistic Heavy Ion Collider (RHIC) at the Brookhaven National Laboratory (BNL).

These results have different interpretations. For instance, the results are consistent with the onset of deconfinement in central Pb+Pb collisions at about  $30A$  GeV [6], assuming that hadron production is mainly determined by the properties of the early stage of the collision. On the other hand, the strangeness horn is also qualitatively described within the thermal model [7, 8], especially when some modifications are considered, see e.g. Refs. [9–11]. Therefore, these data do not allow to make firm conclusions with regard to the onset of deconfinement. The successor of the NA49, the NA61/SHINE Collaboration, is performing the scan of the beam energy and system size at the SPS [12–14]. Additionally, the BES program at RHIC [5] studies Au+Au collisions in the energy range of  $\sqrt{s_{NN}} = 7.7 - 200$  GeV. An important aspect of these studies is a comparison of A+A and p+p collisions. Information about the physical properties of the system created in Pb+Pb and p+p collisions is also very useful in a sense that these reactions represents two limiting cases of the system-sizes.

In the present paper we analyze the new p+p data of the NA61/SHINE at  $p_{\text{lab}} = 20, 31, 40, 80,$  and  $158$  GeV/c [14] (which corresponds to  $\sqrt{s_{NN}} = 6.3, 7.7, 8.8, 12.3, 17.3$  GeV). We also repeat the analysis of the NA49 data in central Pb+Pb collisions. This is done because of an extension of the NA49 data on central Pb+Pb collisions [1–3, 15, 16] in comparison to the results used in previous studies, e.g., in Ref. [17].

We analyze also the recent data from the HADES Collaboration for both p+p collisions at  $E_{\text{kin}} = 3.5$  GeV [18], and Au+Au collisions at  $E_{\text{kin}} = 1.23A$  GeV [19]. The corresponding center of mass energies are  $\sqrt{s_{NN}} = 3.2$  GeV for p+p and  $2.4$  GeV for A+A. For completeness of the analysis we redo the early fits of the Au+Au collisions for  $E_{\text{kin}} = 0.8A, 1.0A$  GeV at GSI Schwerionensynchrotron (SIS), and for the  $E_{\text{lab}} = 11.6A$  GeV at BNL Alternating Gradient Synchrotron (AGS) [20–24]. The corresponding center of mass energies are  $\sqrt{s_{NN}} = 2.2, 2.3,$  and

4.9 GeV.

Therefore, the analyzed energy range is  $\sqrt{s_{NN}} = 3.2 - 17.3$  GeV for p+p interactions and  $\sqrt{s_{NN}} = 2.2 - 17.3$  GeV for central Pb+Pb or Au+Au collisions. Such an analysis extends previous studies regarding the systematic comparison of the hadron production properties in A+A and p+p collisions to energies below  $\sqrt{s_{NN}} = 17.3$  GeV. It should be noted that there are two facilities under construction which will operate in the considered energy region: the Facility for Antiproton and Ion Research (FAIR) [25, 26], and the Nuclotron-based Ion Collider Facility (NICA) [27].

The data on hadron multiplicities are compared with predictions of two popular transport models – Ultra-relativistic Quantum Molecular Dynamics (UrQMD) [28–30] and Hadron String Dynamics (HSD) [31–33]. The properties of p+p interactions are the input to these models. Therefore, we test whether this input obtained from the parametrization of previous p+p results allows to reproduce the new NA61/SHINE data.

We perform the fits of the mean hadron multiplicities within statistical Hadron Resonance Gas (HRG) model in the Grand Canonical Ensemble (GCE) for central Pb+Pb and Au+Au collisions, except for the lowest energies at SIS where the strangeness-canonical ensemble (SCE) was used, and in the Canonical Ensemble (CE) for p+p inelastic interactions. These fits provide us with the HRG model parameters as the functions of collision energy. Particularly, we present a comparison of the chemical freeze-out temperatures in p+p and central collisions of heavy ions in the energy region  $\sqrt{s_{NN}} = 3.2 - 17.3$  GeV. In the literature, such a comparison was previously limited to higher collision energies  $\sqrt{s_{NN}} \geq 19.4$  GeV for p+p [40]. Our results enable one to estimate the range of the chemical freeze-out parameters that can be reached in collisions of different size nuclei during the current energy and system size scanning by NA61/SHINE at SPS, and in the future experiments at NICA and FAIR.

The paper is organized as follows. In Sec. II the results of the calculations of mean hadron multiplicities in inelastic p+p reactions within the UrQMD and HSD models are presented. The HRG is considered in Sec. III. The results for p+p inelastic interactions and central A+A collisions are presented. The summary in Sec. IV closes the paper.

## II. TRANSPORT MODELS FOR PROTON-PROTON COLLISIONS

In this section the UrQMD and HSD transport models results regarding inelastic p+p interactions are compared with the NA61/SHINE data [14] on mean hadron multiplicities  $\langle\pi^+\rangle$ ,  $\langle\pi^-\rangle$ ,  $\langle K^+\rangle$ ,  $\langle K^-\rangle$ , and  $\langle\bar{p}\rangle$  at  $p_{\text{lab}} = 20, 31, 40, 80, 158$  GeV/c which corresponds to  $\sqrt{s_{NN}} = 6.3, 7.7, 8.8, 12.3, 17.3$  GeV (the  $\bar{p}$  multiplicity was not reported for the lowest collision energy). A comparison of the NA61/SHINE results with UrQMD and HSD predictions is presented in Figs. 1 (a)-(e). In addition, the  $\langle K^+\rangle/\langle\pi^+\rangle$  ratio is shown in Fig. 1 (f). From Fig. 1 (a) one con-

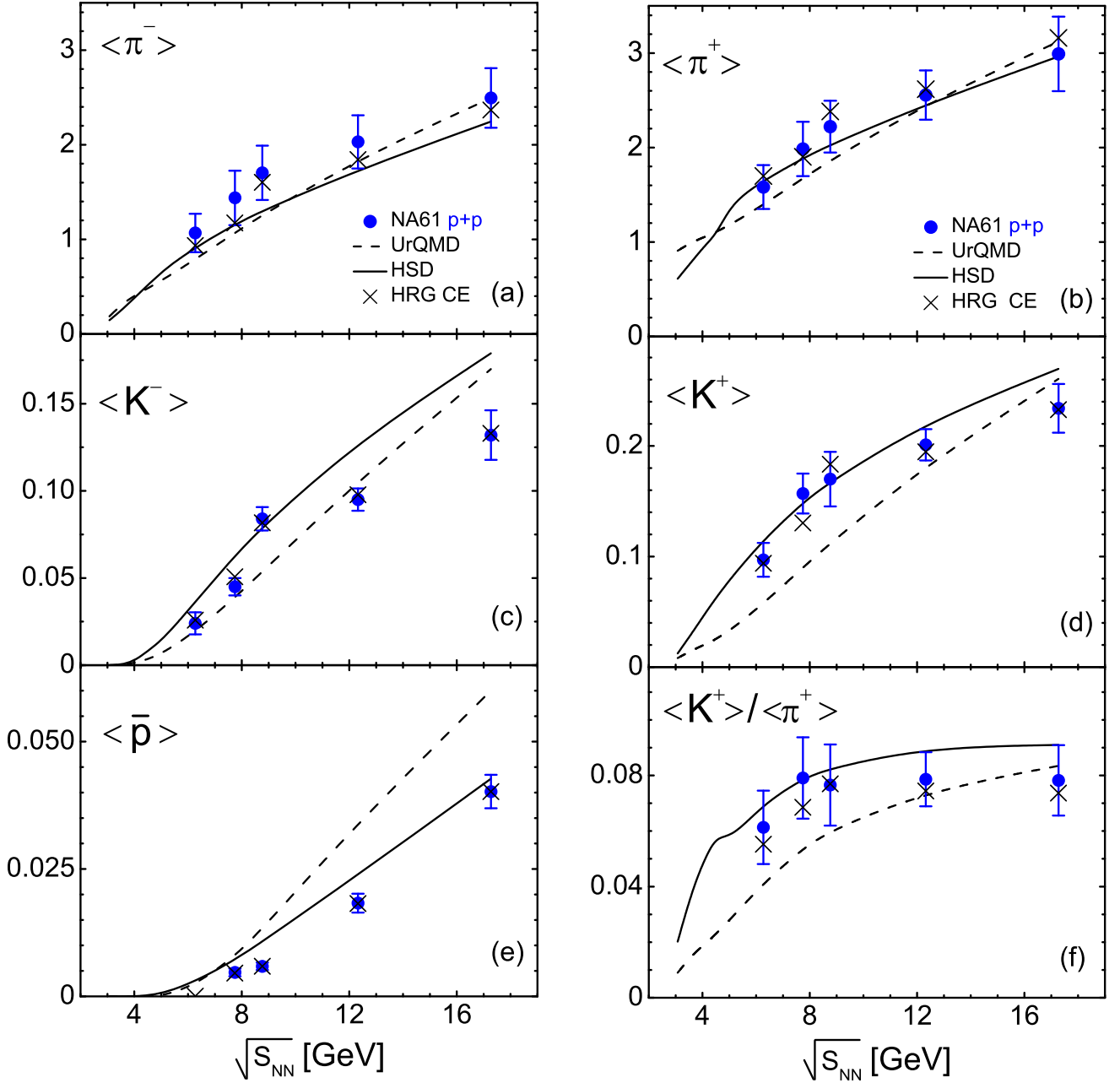


Figure 1: Mean hadron multiplicities in inelastic p+p reactions as functions of the center of mass collision energy  $\sqrt{s_{NN}}$ . The full circles are the data [14] of NA61/SHINE Collaboration. The solid and dashed lines correspond to the results of the HSD 2.5 and UrQMD 3.4 model simulations, respectively. The crosses show the fit in the statistical hadron-resonance gas model in the canonical ensemble (see Sec. III).

cludes that both transport models – UrQMD and HSD – underestimate yields of  $\langle \pi^- \rangle$  at all SPS energies, except the highest one,  $\sqrt{s_{NN}} = 17.3$  GeV. As seen from Figs. 1 (d) and (e) the UrQMD also underestimates  $\langle K^+ \rangle$  and overestimates  $\langle \bar{p} \rangle$ . The both models have problems describing the yields of  $K^-$  shown in Fig. 1 (c). The  $\pi^-$  momentum spectra in p+p reactions within the UrQMD have been analyzed and compared to properly normalized  $\pi^-$  spectra in central Pb+Pb collisions in Ref. [34] (see also Ref. [35], where the mean values of hadron transverse mass have been cal-

culated within the UrQMD and HSD models). It should be noted that the p+p results are used as the input for the transport model description of A+A collisions. Therefore, it is evident that improvements of parametrization of p+p results in both the UrQMD and HSD models are really needed.

### III. HADRON RESONANCE GAS MODEL

#### A. The model formulation

Statistical models appear to be rather successful in calculations of mean hadron multiplicities in high energy collisions. This approach assumes a thermodynamical equilibrium of stable hadrons and resonances at the chemical freeze-out state described by thermal parameters to be determined by fitting data. A general description of the HRG model can be found elsewhere, e.g., in the introduction part of Ref. [36].

In the GCE formulation of the HRG the conserved charges, such as baryonic number  $B$ , electric charge  $Q$ , and net strangeness  $S$ , are conserved on average, but can differ from one microscopic state to another. In the CE formulation these charges are fixed to their exact conserved values in each microscopic state. The distinct difference appears between calculations of hadron multiplicities in different statistical ensembles, if the number of particles with corresponding conserved charge is of the order of unity or smaller [37–42]. In the considered range of collision energies the CE is relevant for p+p collisions, while GCE can be used for central Pb+Pb and Au+Au collisions, except for the lowest energies at SIS. The exact conservation of net strangeness needs to be enforced there, i.e., the calculations for these low-energy A+A collisions are done within the SCE [7, 8].

In the GCE the fitting parameters are the temperature  $T$ , baryonic chemical potential  $\mu_B$ <sup>1</sup>, the system volume  $V$ , and the strangeness under-saturation parameter  $\gamma_S$  which is discussed in Ref. [43]. For the convenient comparison between A+A and p+p we use the radius  $R$  calculated from  $V \equiv 4\pi R^3/3$  instead of volume. The CE treatment of p+p collisions assumes the fixed values of the conserved charges – baryonic number  $B = 2$ , electric charge  $Q = 2$ , and net strangeness  $S = 0$ . Therefore, in the CE the fitting parameters are  $T$ ,  $R$ , and  $\gamma_S$ . In the SCE for SIS we set the strangeness conservation radius equal to the radius of the system. Therefore, the fit parameters in the SCE are the same as in the CE, but only strangeness is conserved exactly. Note that at low collision energies a role of the exact energy conservation becomes quite important. One should

---

<sup>1</sup> The chemical potentials  $\mu_S$  and  $\mu_Q$  correspond to the conservation of strangeness and electric charge, respectively. They are found from the conditions of zero net strangeness and fixed proton to neutron ratio in the colliding nuclei.

then follow the micro canonical ensemble formulation which has not been used in the present paper.

The HRG model fits are done by minimizing the value

$$\frac{\chi^2}{N_{\text{dof}}} = \frac{1}{N_{\text{dof}}} \sum_{i=1}^N \frac{(N_i^{\text{exp}} - N_i^{\text{HRG}})^2}{\sigma_i^2}, \quad (1)$$

where  $N_i^{\text{exp}}$  and  $N_i^{\text{HRG}}$  are the experimental and calculated in the HRG hadron multiplicities, respectively;  $N_{\text{dof}}$  is the number of degrees of freedom, that is the number of the data points minus the number of fitting parameters; and  $\sigma_i^2 = (\sigma_i^{\text{sys}})^2 + (\sigma_i^{\text{stat}})^2$  is the sum of the squares of the statistical and systematic experimental errors.

In our calculations we include stable hadrons and resonances that are listed by the Particle Data Group [44], and take into account both the quantum statistics, and the Breit-Wigner shape of resonances with finite widths. The list of particles includes mesons up to  $f_2(2340)$ , (anti-)baryons up to  $N(2600)$ , and generally corresponds to the newest THERMUS 3.0 [36] compilation. We do not include hadrons with charm and bottom degrees of freedom which have a negligible effect on the fit results. In contrast to the Refs. [9, 10] we also removed the  $\sigma$  meson ( $f_0(500)$ ) and the  $\kappa$  meson ( $K_0^*(800)$ ) from the particle list because of the reasons explained in Refs. [45–48].

The mean multiplicity  $\langle N_i \rangle$  of  $i$ th particle species is calculated in the HRG model as a sum of the primordial mean multiplicity  $\langle N_i^{\text{prim}} \rangle$  and resonance decay contributions as follows

$$\langle N_i \rangle = \langle N_i^{\text{prim}} \rangle + \sum_R \langle n_i \rangle_R \langle N_R^{\text{prim}} \rangle, \quad (2)$$

where  $\langle n_i \rangle_R$  is the average number of particles of type  $i$  resulting from decay of resonance  $R$ . Note that Eq. (2) is also valid for calculating yields of unstable particles, such as the  $\phi$  meson,  $K^*(892)$  resonance, or  $\Lambda(1520)$  resonance. This is important since yields of these unstable particles have been measured (see, e.g. Ref. [15, 16, 18, 49]). Note, however, that the present version of THERMUS does not take into account the resonance decay contribution to mean multiplicities of particles which are marked as unstable. As a result, yields of  $\phi$ ,  $K^*(892)$ , or  $\Lambda(1520)$  can be underestimated by up to 25%. The actual amount depends on the HRG parameters used, and on the modeling of relevant decay branching ratios, which are sometimes poorly constrained. On the other hand, if, e.g., one marks the  $\phi$  as a stable particle in THERMUS, then the decay contribution to the  $\phi$  multiplicity is calculated, but the further decays of  $\phi$  to kaons or pions are not taken into account in the program, while they are accounted in the experiment. To avoid this problem and to simultaneously fit yields of stable and unstable hadrons in THERMUS one has to use multiple particle sets. Alternatively, one can add an extra loop for the summation of the decay contributions to the yields of unstable particles in the THERMUS code.

We have verified that in this case THERMUS yields essentially the same results for total hadron yields of all particles as our own implementation of the HRG. Thus, we use the latter in all our

subsequent analysis. We also enable the calculation of asymmetric error bars for the obtained parameters, which are obtained by explicitly analyzing the  $\chi^2 = \chi_{\min}^2 + 1$  contours.

## B. HRG results for central A+A collisions and p+p inelastic reactions

The A+A data at AGS and SPS energies are fitted within the GCE HRG model. The SCE HRG formulation is employed to describe the old A+A data at SIS (marked as SIS in the figures), and the new data obtained at SIS by HADES (marked as HADES). The p+p data of HADES and NA61/SHINE collaborations are analyzed within the CE HRG. The extracted values of the chemical freeze-out parameters,  $T$  and  $\mu_B$ , are plotted in Fig. 2 (a). The boxes correspond to our fit of the latest compilation of the NA49 data for central Pb+Pb collisions [1–3, 15, 16]. The full right triangles show our fit to the recent Au+Au data from HADES [19]. The open right triangles show the results of the newest analysis of the p+Nb and Ar+KCl reactions performed using THERMUS 3.0 by the HADES collaboration [50]. The Ar+KCl\* label corresponds to the fit with the reduced number of fitted yields [50]. The up and down triangles show our fits to the old Au+Au data listed in [21] and in [24]. The Au+Au data at SIS allow to extract temperature and baryonic chemical potential. They are shown in Figs. 2 (a) and (b). The parameters  $R$  and  $\gamma_S$  however can not be reliably defined, thus, they are not shown in Fig. 2 (c) and 2 (d) at SIS.

The main set of data used in our analysis contains the mean total multiplicities. All the data from the NA61/SHINE, NA49 at SPS, and also the point at AGS energy are the total  $4\pi$  mean multiplicities, i.e., the hadron yields integrated over the whole rapidity range. The p+p data from HADES are also the mean multiplicities, but extracted from di-electron yields, which may add some unaccounted systematic error to this point. The SIS Au+Au data contains the hadron yield ratios and the average number of participants. The Au+Au data from HADES contains only the ratios at mid-rapidity. The HRG model parameters obtained from different sets of data demonstrate the smooth and consistent behavior. The largest deviation is seen at the  $\sqrt{s_{NN}} = 6.3$  GeV in p+p reactions from the NA61/SHINE. This can be attributed to the absence of the antiproton data at  $\sqrt{s_{NN}} = 6.3$  GeV, which are present in the measurements at four higher SPS energies provided by the same collaboration.

The grey band in Fig. 2 (a) is the parametrization from the Ref. [51],

$$T_{A+A}(\mu_B) = a - b\mu_B^2 - c\mu_B^4, \quad (3)$$

where  $a = 0.166 \pm 0.002$  GeV,  $b = 0.139 \pm 0.016$  GeV<sup>-1</sup>, and  $c = 0.053 \pm 0.021$  GeV<sup>-3</sup>. The width of the band indicates the corresponding error bars, that were obtained for each  $T(\mu_B)$  point from the errors of the  $a$ ,  $b$  and  $c$ , using the standard methods of propagations of uncertainties. Together

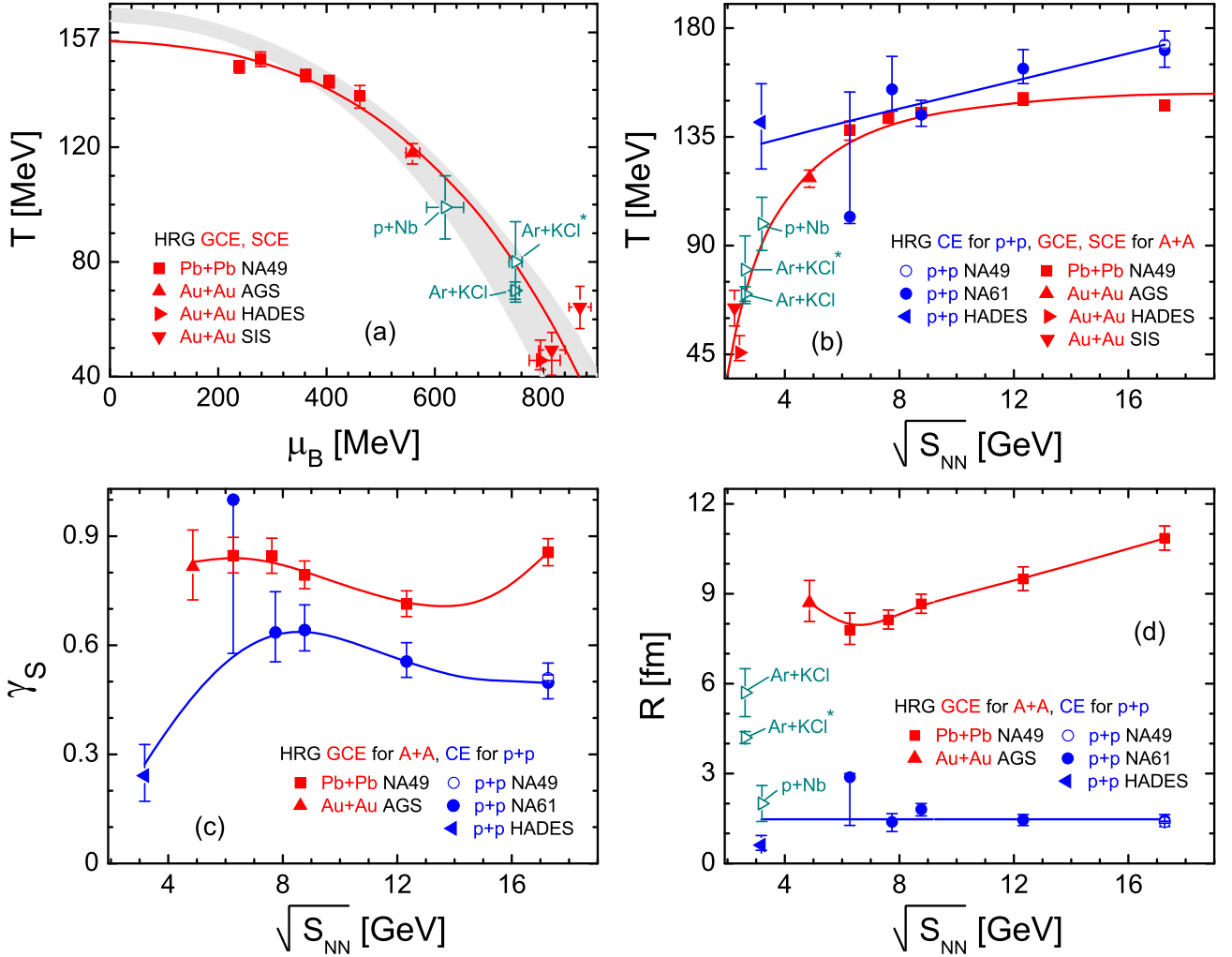


Figure 2: (a) Temperature  $T$  as a function of baryon chemical potential in central Pb+Pb and Au+Au collisions. Temperature  $T$  (b), strangeness saturation factor  $\gamma_S$  (c), radius of the system  $R$  (d) in p+p inelastic reactions and central heavy ion collisions as functions of the collision energy, see text for more explanations.

with the parametrization of the  $\mu_B$ ,

$$\mu_B = \frac{d}{1 + e\sqrt{s_{NN}}}, \quad (4)$$

where  $d = 1.308 \pm 0.028$  GeV,  $e = 0.273 \pm 0.008$  GeV $^{-1}$ , Eq. (3) allows to plot temperature as the function of energy.

The fit of our results for  $T$  and  $\mu_B$  in central Pb+Pb and Au+Au collisions with the same analytical functions (3) and (4) yields somewhat different parameters, namely:  $a = 0.157$  GeV,  $b = 0.087$  GeV $^{-1}$ ,  $c = 0.092$  GeV $^{-3}$ ,  $d = 1.477$  GeV,  $e = 0.343$  GeV $^{-1}$ . The corresponding error bars are rather large and are not shown, because we used only a few points to determine the freeze-out line. However, the obtained line in Fig. 2 (a) is within the gray error bars at large chemical potential. Therefore adding new points there would not change the line. The most important



effect is due to the top SPS points that give smaller temperature in our analysis. Interestingly, Eq. (3) gives  $T = 157$  MeV at  $\mu_B = 0$ , which is close to the latest findings at the LHC [52–54].

The change in the parametrization of the chemical freeze-out line (3) and (4) is a combination of two effects: the extension of the list of particles, and the changes in the experimentally measured particle set. The HRG fit of the latest NA49 data [1–3, 15, 16] in the present paper gives approximately constant temperature at top SPS energies and growing radius of the system, as seen from Figs. 2 (b) and (d). The previous HRG fit [17] of the old NA49 data with a smaller table of particles in the HRG gave the opposite: constant radius and growing temperature.

In order to further study the effects of heavy resonance decays on the HRG model parameters, we have analyzed different cuts for the maximal resonance mass,  $M_{\text{cut}}$ , included in the table of particles. Varying the cut in the range  $1.7 < M_{\text{cut}} < 2.4$  GeV, we have found that the inclusion of heavy resonances may decrease the temperature up to 10 MeV, and the effect is stronger for larger collision energy.

The data of the NA61/SHINE on inelastic p+p interactions [14] are fitted in the CE HRG model. The experimental results and HRG fit within the CE are shown in Fig. 1 and in Tables I and II. The obtained  $T$ ,  $\gamma_S$ , and  $R$  parameters are presented in Table III. These parameters are also shown in Figs. 2 (b-d) for both p+p and A+A collisions.

In addition, we make the fit of the available p+p data point from the NA49 at the  $E_{\text{lab}} = 158$  GeV ( $\sqrt{s_{NN}} = 17.3$  GeV) [16, 49]. The NA49 p+p data include more hadron species, therefore, we check how the selection of a different particle set influences the results. We also fit the data from HADES Collaboration [18], for p+p collisions at  $E_{\text{kin}} = 3.5$  GeV ( $\sqrt{s_{NN}} = 3.2$  GeV).

The lower solid line in Fig. 2 (b) shows the behavior of temperature in A+A as the function of energy calculated according to Eqs. (3) and (4). Other lines in Figs.2 (b)-(d) are the fits that were made to guide the eye.

The analysis of the NA49 and NA61/SHINE p+p data at 158A GeV gives very close HRG parameters. The corresponding points almost coincide. Larger error bars for the NA61/SHINE are due to smaller number of measured particles compared to NA49 (5 versus 18). The same reason causes much smaller  $\chi^2/N_{\text{dof}}$  for NA61/SHINE than that for NA49. The extracted freeze-out parameters are only slightly changed by adding the new multiplicity data to the NA61/SHINE set of particles measured at 158A GeV. The further addition of the particles leads only to an increase of the  $\chi^2/N_{\text{dof}}$  and decrease of the error bars, i.e., the larger number of fitted particles gives more constraints on the range of the HRG parameters.

It is seen from Table III that values of  $\chi^2/N_{\text{dof}}$  are significantly smaller than unity for collision energies  $\sqrt{s_{NN}} = 8.8, 12.3, 17.3$  GeV. This usually indicates that the experimental errors might be overestimated.

Table I: The comparison between fitted and measured total  $4\pi$  multiplicities, and the prediction for the unmeasured yields. The fit is done within the CE formulation of the HRG. Some yields at the lowest energy are omitted from the table, because the energy of the system is not enough for their creation. The mean multiplicities in p+p inelastic interactions are measured by HADES [18] at  $\sqrt{s_{NN}} = 3.2$  GeV, and by NA61/SHINE [14] at  $\sqrt{s_{NN}} = 6.3$  GeV and 7.7 GeV.

	$\sqrt{s_{NN}} = 3.2$ GeV		$\sqrt{s_{NN}}=6.3$ GeV		$\sqrt{s_{NN}} =7.7$ GeV	
	Measurement	Fit	Measurement	Fit	Measurement	Fit
$\pi^+$		0.782	$1.582 \pm 0.232$	1.698	$1.985 \pm 0.288$	1.903
$\pi^-$		0.238	$1.067 \pm 0.203$	0.9345	$1.438 \pm 0.288$	1.174
$K^+$		0.00398	$0.097 \pm 0.015$	0.0938	$0.157 \pm 0.018$	0.130
$K^-$		$3.82 \cdot 10^{-4}$	$0.024 \pm 0.00632$	0.0258	$0.045 \pm 0.005$	0.051
$p$		1.37		1.14		1.1
$\bar{p}$		–		$4.78 \cdot 10^{-5}$	$0.0047 \pm 0.0008$	0.0046
$\Lambda$		0.00466		0.0669		0.0785
$\bar{\Lambda}$		–		$1.57 \cdot 10^{-5}$		0.00161
$\Sigma^+$		$2.20 \cdot 10^{-4}$		0.0226		0.0254
$\bar{\Sigma}^+$		–		$3.11 \cdot 10^{-6}$		$3.27 \cdot 10^{-4}$
$\Sigma^-$		$6.00 \cdot 10^{-5}$		0.011		0.0129
$\bar{\Sigma}^-$		–		$4.78 \cdot 10^{-6}$		$4.90 \cdot 10^{-4}$
$\Xi^0$		–		$9.04 \cdot 10^{-4}$		0.00122
$\bar{\Xi}^0$		–		$7.35 \cdot 10^{-7}$		$8.32 \cdot 10^{-5}$
$\Xi^-$		–		$6.93 \cdot 10^{-4}$		0.00101
$\bar{\Xi}^-$		–		$8.53 \cdot 10^{-7}$		$9.36 \cdot 10^{-5}$
$\Omega$		–		$4.06 \cdot 10^{-6}$		$1.11 \cdot 10^{-5}$
$\bar{\Omega}$		–		$1.70 \cdot 10^{-8}$		$3.28 \cdot 10^{-6}$
$\pi^0$	$0.39 \pm 0.1$	0.578		1.54		1.76
$K_S^0$	$0.0013 \pm 0.0003$	0.000977		0.0501		0.0811
$\eta$	$0.02 \pm 0.007$	0.017		0.0846		0.134
$\omega$	$0.006 \pm 0.002$	0.00591		0.0364		0.145
$K^{*+}$	$(2.0 \pm 0.6) \cdot 10^{-4}$	0.000218		0.0113		0.0406
$K^{*-}$		$4.62 \cdot 10^{-5}$		0.00273		0.0117
$K^{*0}$		$1.36 \cdot 10^{-4}$		0.00797		0.0302
$K^{*-0}$		$5.86 \cdot 10^{-5}$		0.00347		0.0144
$\phi$		$7.72 \cdot 10^{-5}$		0.00454		0.0129
$\Lambda(1520)$		$3.83 \cdot 10^{-5}$		0.00206		0.00626

Table II: The same as Table I for p+p inelastic interactions at  $\sqrt{s_{NN}}=8.8, 12.3,$  and  $17.3$  GeV measured by NA61/SHINE [14].

	$\sqrt{s_{NN}}=8.8$ GeV		$\sqrt{s_{NN}}=12.3$ GeV		$\sqrt{s_{NN}}=17.3$ GeV	
	Measurement	Fit	Measurement	Fit	Measurement	Fit
$\pi^+$	$2.221 \pm 0.274$	2.383	$2.556 \pm 0.261$	2.618	$2.991 \pm 0.394$	3.161
$\pi^-$	$1.703 \pm 0.287$	1.603	$2.030 \pm 0.281$	1.844	$2.494 \pm 0.315$	2.368
$K^+$	$0.170 \pm 0.025$	0.183	$0.201 \pm 0.014$	0.195	$0.234 \pm 0.022$	0.233
$K^-$	$0.084 \pm 0.007$	0.081	$0.095 \pm 0.006$	0.098	$0.132 \pm 0.014$	0.133
$p$		1.05		1.04		1.04
$\bar{p}$	$0.0059 \pm 0.0007$	0.0059	$0.0183 \pm 0.00186$	0.0182	$0.0402 \pm 0.0033$	0.0402
$\Lambda$		0.0987		0.0974		0.104
$\bar{\Lambda}$		0.00196		0.00553		0.0108
$\Sigma^+$		0.0314		0.0301		0.0314
$\bar{\Sigma}^+$		$4.19 \cdot 10^{-4}$		0.00118		0.00237
$\Sigma^-$		0.018		0.0179		0.0202
$\bar{\Sigma}^-$		$5.90 \cdot 10^{-4}$		0.00164		0.00315
$\Xi^0$		0.00203		0.00198		0.0023
$\bar{\Xi}^0$		$1.02 \cdot 10^{-4}$		$2.70 \cdot 10^{-4}$		$4.91 \cdot 10^{-4}$
$\Xi^-$		0.00171		0.00171		0.00204
$\bar{\Xi}^-$		$1.13 \cdot 10^{-4}$		$2.95 \cdot 10^{-4}$		$5.28 \cdot 10^{-4}$
$\Omega$		$2.31 \cdot 10^{-5}$		$2.59 \cdot 10^{-5}$		$3.47 \cdot 10^{-5}$
$\bar{\Omega}$		$3.77 \cdot 10^{-6}$		$1.03 \cdot 10^{-5}$		$1.80 \cdot 10^{-5}$
$\pi^0$		2.28		2.53		3.12
$K_S^0$		0.122		0.137		0.174
$\eta$		0.173		0.204		0.256
$\omega$		0.185		0.253		0.343
$K^{*+}$		0.0519		0.0647		0.0804
$K^{*-}$		0.019		0.026		0.0377
$K^{*0}$		0.0403		0.0517		0.0665
$\bar{K}^{*0}$		0.0227		0.0305		0.0432
$\phi$		0.0157		0.0183		0.0211
$\Lambda(1520)$		0.00707		0.00853		0.00978

Table III: Summary of the fitted parameters in p+p inelastic interactions within CE formulation of HRG.

Parameters	$\sqrt{s_{NN}}=3.2$ GeV	$\sqrt{s_{NN}}=6.3$ GeV	$\sqrt{s_{NN}}=7.7$ GeV
$T$ (MeV)	$141.0^{+15.9}_{-19.3}$	$102.0^{+51.6}_{-2.8}$	$154.6^{+13.6}_{-8.9}$
$\gamma_S$	$0.242^{+0.086}_{-0.071}$	$1.000^{+0.000}_{-0.423}$	$0.635^{+0.112}_{-0.081}$
$R$ (fm)	$0.61^{+0.32}_{-0.17}$	$2.88^{+0.12}_{-1.61}$	$1.38^{+0.28}_{-0.32}$
$\chi^2/N_{\text{dof}}$	4.95/2	0.80/1	4.44/2
	$\sqrt{s_{NN}}=8.8$ GeV	$\sqrt{s_{NN}}=12.3$ GeV	$\sqrt{s_{NN}}=17.3$ GeV
$T$ (MeV)	$144.1^{+5.9}_{-4.8}$	$163.3^{+7.9}_{-6.2}$	$170.8^{+8.0}_{-7.0}$
$\gamma_S$	$0.642^{+0.069}_{-0.058}$	$0.555^{+0.052}_{-0.043}$	$0.497^{+0.053}_{-0.045}$
$R$ (fm)	$1.80^{+0.20}_{-0.21}$	$1.46^{+0.18}_{-0.19}$	$1.44^{+0.19}_{-0.21}$
$\chi^2/N_{\text{dof}}$	0.89/2	0.88/2	0.35/2

The temperature in p+p is gradually increasing with collision energy from  $T_{\text{p+p}} \simeq 130$  MeV to  $T_{\text{p+p}} \simeq 170$  MeV. The sudden drop of the temperature at  $\sqrt{s_{NN}} = 6.3$  GeV is correlated with the corresponding increase of the radius  $R_{\text{p+p}}$  and the  $\gamma_S$ . Large error bars at this energy indicate that the measurement of the  $\bar{p}$  and/or other (anti)baryon is needed to constrain the parameters.

The HRG model for multiplicities in p+p reactions at  $\sqrt{s_{NN}} = 19.4$  GeV was considered in Ref. [39, 40]. This energy is close to the top SPS energy. The p+p temperature in Ref. [39, 40] is in agreement with our results within the error bars. The  $e^+e^-$  and p+ $\bar{p}$  temperatures in Ref. [39, 40] are also close to our results. The p+p temperature for  $\sqrt{s_{NN}} = 200$  GeV at RHIC was found to be  $T_{\text{p+p}} \simeq 170$  MeV [55], which is in agreement with a slow increase and a saturation of the temperature obtained in our fit.

A possible universal mechanism of thermal hadron production in collisions of elementary particles was suggested in Ref. [56]. It connects the temperature to the string tension between quarks, and explains why the temperatures in  $e^+e^-$ , p+p, and p+ $\bar{p}$  appear to be close to each other. On the other hand, secondary collisions and medium effects are evidently important in central Pb+Pb (or Au+Au) collisions.

The unexpected finding is a decrease of  $\gamma_S$  parameter with collision energy in p+p inelastic reactions in the SPS energy region. Together with the point from HADES one may conclude that  $\gamma_S$  increases at small energies and probably has a maximum at the low SPS energy. As seen from Fig. 2 (c) a similar behavior is observed for  $\gamma_S$  in central Pb+Pb and Au+Au collisions. Our results at the top SPS energy agree with those obtained in Ref. [39, 40]. We note that previous studies on hadron production in p+p collisions dealt with higher collision energies than those considered in our paper. There the  $\gamma_S$  parameter was generally found to increase with collision energy. Our results at SPS energies are also in a slight contrast with recent paper [57], where it is

implied that  $\gamma_S$  universally increases with collision energy. However, the corresponding error bars are still large to make the final conclusions.

As seen from Fig. 2 (d) the system radius in p+p inelastic reactions is approximately independent of the collisions energy,  $R_{p+p} \simeq 1.5$  fm. An exception is the lowest energy p+p point from HADES. The volume that was found in the p+p reactions at RHIC gives essentially larger values of the radius,  $R_{p+p} \simeq 3.6$  fm [55]. We do not see, however, the increase of  $R$  at the SPS energies. The dependence of the radius on the collision energy is rather different in p+p and A+A collisions at the SPS energies: it grows in central A+A collisions, while in p+p inelastic reactions the radius is approximately constant.

Note that the excluded volume corrections [58] neglected in the present paper do not change the results for the intensive HRG model parameters –  $T$ ,  $\mu_B$ ,  $\gamma_S$  – only if all hard-core radii of hadrons are assumed to be equal to each other. However, the excluded volume corrections can significantly reduce the densities [59] and, thus, increase the total system volume at chemical freeze-out in a comparison to the ideal HRG. Therefore, the finite size of hadrons influences the total system volume: the values of  $R_{p+p}$  and  $R_{A+A}$  would become larger and their energy dependence would be changed. The intensive HRG model parameters can also be influenced, if one considers hadrons with different hard-core radii [60, 61]. However, this will require additional assumptions (and new model parameters) about sizes of various hadrons, which are presently rather poorly constrained.

Thermal HRG model parameters for all intermediate systems like p+A or A+A collisions of small nuclei are expected to be in between those found in the present study for Pb+Pb and p+p reactions. Presently existing results, particularly, the independent analysis of p+Nb and Ar+KCl reactions by HADES Collaboration [50] supports this statement. The existing results also indicate that temperatures reached by different systems in the beam energy scan at the SPS might be very similar. However, exact conservation of net strangeness and baryonic number remains important in p+A and light nuclei collisions. Therefore, the total number of strange hadrons and antibaryons per nucleon participant may be essentially reduced for small systems despite of their larger temperatures.

#### IV. SUMMARY

Our analysis of the new data for mean hadron multiplicities demonstrates that both transport models – UrQMD and HSD – should be significantly modified and tuned to the presently available p+p data at SPS energies. This is indeed important as the properties of p+p reactions are used in these transport models as the input for Monte Carlo simulations of A+A collisions.

The CE HRG model leads to the good description of the data on hadron multiplicities in p+p interactions. Our results define the range of the chemical freeze-out parameters –  $T$ ,  $\gamma_S$ , and  $R$  –

that can be reached in collisions of different size nuclei during the energy and system size scanning at the SPS energy range. The comparison of the obtained HRG parameters in p+p inelastic reactions and central Pb+Pb (or Au+Au) collisions shows that the freeze-out temperature in p+p is larger than that in A+A,  $T_{p+p} > T_{A+A}$ . The temperature in p+p slowly grows with energy from 130 to 170 MeV, while the A+A temperature strongly increases at small collision energy and saturates fast at  $T_{A+A} \simeq 157$  MeV, in contrast to  $T_{A+A} \simeq 166$  MeV found in previous studies. In the considered energy range the largest difference  $T_{p+p} - T_{A+A} \cong 60$  MeV is at low energies. The  $T_{p+p} \simeq T_{A+A}$  at  $\sqrt{s_{NN}} = 6.3 - 7.7$  GeV, and then the difference grows again reaching about 20 MeV at the highest SPS energy.

At all collision energies the  $\gamma_S$  parameter in central Pb+Pb and Au+Au collisions is larger than that in p+p inelastic reactions. It seems that in both cases this parameter has a local maximum at the low SPS energy. The obtained results also indicate that  $\gamma_S$  parameter in p+p interactions decreases with collision energy at SPS energies. While the error bars are still too large to make firm conclusions, this is in contrast with the previous studies, which dealt with higher collision energies, and predicted a monotonous increase of the  $\gamma_S$  with the collision energy.

The dependence of the system radius on the collision energy is rather different in central Pb+Pb collisions and p+p reactions in the SPS energy region. The radius  $R_{A+A}$  increases with collision energy for 40%, while  $R_{p+p}$  has approximately constant value. The  $R_{A+A}$  dependence found in our analysis is different than in the previous studies<sup>2</sup>, where  $R_{A+A}$  was approximately constant at the SPS. The radius, temperature, and the  $\gamma_S$  parameters in p+p reactions at such low collision energies are obtained for the first time.

The fit of the mean multiplicities considered in the present paper, both in p+p and A+A reactions, assumes that a system behaves at the chemical freeze-out as the ideal hadron resonance gas. Thus, the effects of the possible deconfinement phase transition may be signaled as some irregular behavior of the obtained parameters and deviations of the data from the HRG model results. We do see an indication of such an irregular behavior for  $\gamma_S$  at low energies in A+A collisions and, surprisingly, even stronger in p+p interactions. However, there is not enough data at low energy A+A, while the lowest available p+p point contains a different set of measured particles than for other p+p points. Therefore, the uncertainties in extracted parameters are still too large to make firm conclusions and more data in both A+A and p+p are needed at this energy range in order to clarify this point.

The measurements of total particle multiplicities for a wider set of hadron species are needed. The minimal set of fitted multiplicities should include particles possessing all three conserved

---

<sup>2</sup> It should be noted that finite size of hadrons, neglected in the present paper, may have an influence on the total system volume and its dependence on the collision energy.

charges  $-B$ ,  $S$ ,  $Q$  – and the corresponding anti-particles for both p+p and A+A. For example, an appropriate set of hadron species may include  $\pi^+$ ,  $\pi^-$ ,  $K^+$ ,  $K^-$ ,  $p$ , and  $\bar{p}$ . Therefore, the additional measurements of anti-proton at the lowest SPS and proton mean multiplicities in both p+p and intermediate A+A reactions at all SPS energies are necessary.

### Acknowledgments

We are thankful to M. Gazdzicki and S. Pulawski for fruitful comments, and to J. Cleymans and S. Wheaton for the clarification of decay contributions to the hadron yields in THERMUS. We thank NA49, NA61/SHINE, and HADES Collaborations for providing us the data. V.V.B. thanks for support by Polish National Science Center grant No. DEC-2012/06/A/ST2/00390. The work of M.I.G. was supported by the Program of Fundamental Research of the National Academy of Sciences of Ukraine.

- 
- [1] S.V. Afanasiev *et al.* [NA49 collaboration], Phys. Rev. C **66**, 054902 (2002).
  - [2] C. Alt *et al.* [NA49 Collaboration], Phys. Rev. C **73**, 044910 (2006).
  - [3] C. Alt *et al.* [NA49 collaboration], Phys. Rev. C **77**, 024903 (2008).
  - [4] M. Gazdzicki and M. I. Gorenstein, Acta Phys. Polon. **B30**, 2705 (1999).
  - [5] M. M. Aggarwal *et al.* [STAR Collaboration], arXiv:1007.2613 [nucl-ex]; S. Das [STAR Collaboration], EPJ Web Conf. **90**, 08007 (2015) doi:10.1051/epjconf/20159008007 [arXiv:1412.0499 [nucl-ex]].
  - [6] M. Gazdzicki, M. I. Gorenstein, and P. Seyboth, Acta Phys. Polon. **B42**, 307 (2011); Int. Journ. Mod. Phys. E **23**, 1430008 (2014) [arXiv:1404.3567 [nucl-ex]].
  - [7] P. Braun-Munzinger, J. Cleymans, H. Oeschler, and K. Redlich, Nucl. Phys. A **697**, 902 (2002).
  - [8] J. Cleymans, B. Hippolyte, H. Oeschler, K. Redlich and N. Sharma, arXiv:1603.09553 [hep-ph].
  - [9] A. Andronic, P. Braun-Munzinger, and J. Stachel, Phys. Lett. B **673**, 142 (2009).
  - [10] D. R. Oliinychenko, K. A. Bugaev and A. S. Sorin, Ukr. J. Phys. **58**, no. 3, 211 (2013) [arXiv:1204.0103 [hep-ph]].
  - [11] M. Naskret, D. Blaschke and A. Dubinin, Phys. Part. Nucl. **46**, no. 5, 789 (2015) [arXiv:1501.01599 [hep-ph]].
  - [12] M. Gaździcki [NA61/SHINE Collaboration], J. Phys. G **36**, 064039 (2009).
  - [13] N. Abgrall *et al.* [NA61 Collaboration], JINST **9** (2014) P06005.
  - [14] N. Abgrall *et al.* [NA61/SHINE Collaboration], Eur. Phys. J. C **74** (2014) 3, 2794; S. Pulawski [NA61/SHINE Collaboration], PoS CPOD **2014** (2015) 010; A. Aduszkiewicz [NA61/SHINE Collaboration], CERN-SPSC-2015-036; SPSC-SR-171, [http://cds.cern.ch/record/2059310].

- [15] C. Alt *et al.* [NA49 Collaboration], Phys. Rev. C **78**, 034918 (2008); C. Alt *et al.*, Phys. Rev. C **78**, 044907 (2008); C. Alt *et al.*, Phys. Rev. Lett. **94**, 192301 (2005); T. Anticic *et al.*, Phys. Rev. C **85**, 044913 (2012); V. Friese, Nucl. Phys. A **698**, 487 (2002); see also [<https://edms.cern.ch/document/1075059/4>].
- [16] T. Anticic *et al.*, Phys. Rev. C **84**, 064909 (2011).
- [17] F. Becattini, J. Manninen and M. Gazdzicki, Phys. Rev. C **73**, 044905 (2006).
- [18] G. Agakishiev *et al.* [HADES Collaboration], Phys. Lett. B **715**, 304 (2012); Eur. Phys. J. A **48**, 64 (2012); Phys. Rev. C **90**, 015202 (2014); Phys. Rev. C **92**, 024903 (2015).
- [19] M. Lorenz [HADES Collaboration], Nucl. Phys. A **931**, 785 (2014).
- [20] J. Cleymans, H. Oeschler and K. Redlich, Phys. Rev. C **59**, 1663 (1999).
- [21] R. Auerbeck, R. Holzmann, V. Metag, and R. S. Simon, Phys. Rev. C **67**, 024903 (2003).
- [22] L. Ahle *et al.*, [E-802 Collaboration], Phys. Rev. C **59**, 2173 (1991); Phys. Rev. C **60**, 044904 (1999); Phys. Rev. C **60**, 064901 (1999).
- [23] S. Ahmad *et al.*, Phys. Lett. B **382**, 35 (1996); S. Albergo *et al.*, Phys. Rev. Lett. **88**, 062301 (2002).
- [24] F. Becattini, J. Cleymans, A. Keranen, E. Suhonen, and K. Redlich, Phys. Rev. C **64**, 024901 (2001).
- [25] B. Friman, C. Hohne, J. Knoll, S. Leupold, J. Randrup, R. Rapp, and P. Senger, Lect. Notes Phys. **814**, 1 (2011).
- [26] P. Senger [CBM Collaboration], Cent. Eur. J. Phys., **10**, 1289 (2012).
- [27] NICA White Paper [<http://theor0.jinr.ru/twiki/cgi/view/NICA/WebHome>].
- [28] S. A. Bass *et al.*, Prog. Part. Nucl. Phys. **41**, 255 (1998); M. Bleicher *et al.*, J. Phys. G **25**, 1859 (1999).
- [29] H. Petersen, M. Bleicher, S.A. Bass, and H. Stöcker, arXiv:0805.0567 [hep-ph].
- [30] UrQMD 3.4 code is available at [<http://urqmd.org/>].
- [31] W. Ehehalt and W. Cassing, Nucl. Phys. A **602**, 449 (1996).
- [32] J. Geiss, W. Cassing and C. Greiner, Nucl. Phys. A **644**, 107 (1998).
- [33] W. Cassing and E. L. Bratkovskaya, Phys. Rept. **308**, 65 (1999).
- [34] V.Yu. Vovchenko, D.V. Anchishkin, and M.I. Gorenstein, Phys. Rev. C **90**, 024916 (2014).
- [35] V.Yu. Vovchenko, D.V. Anchishkin, and M.I. Gorenstein, Nucl. Phys. A **936**, 1 (2015).
- [36] S. Wheaton, J. Cleymans, and M. Hauer, Comput. Phys. Commun. **180**, 84 (2009).
- [37] J. Rafelski and M. Danos, Phys. Lett. B **97**, 279 (1980).
- [38] J. Cleymans, K. Redlich, and E. Suhonen, Z. Phys. C **51**, 137 (1991).
- [39] F. Becattini, Z. Phys. C **69**, 485 (1996) and Nucl. Phys. Proc. Suppl. **92**, 137 (2001).
- [40] F. Becattini and U. W. Heinz, Z. Phys. C **76**, 269 (1997); [Z. Phys. C **76**, 578 (1997)].
- [41] M.I. Gorenstein, M. Gaździcki and W. Greiner, Phys. Lett. B **483**, 60 (2000); M.I. Gorenstein,



- A. P. Kostyuk, H. Stöcker, and W. Greiner, Phys. Lett. B **509**, 277 (2001); M.I. Gorenstein, W. Greiner, and A. Rustamov, Phys. Lett. B **731**, 302 (2014).
- [42] V. V. Begun, L. Ferroni, M. I. Gorenstein, M. Gazdzicki, and F. Becattini, J. Phys. G **32**, 1003 (2006).
- [43] J. Rafelski, Eur. Phys. J. A **51**, 114 (2015).
- [44] K. A. Olive *et al.* [Particle Data Group Collaboration], Chin. Phys. C **38**, 090001 (2014).
- [45] R. Venugopalan and M. Prakash, Nucl. Phys. A **546**, 718 (1992).
- [46] A. Gomez Nicola, J. R. Pelaez, and J. R. de Elvira, Phys. Rev. D **87**, 016001 (2013).
- [47] W. Broniowski, F. Giacosa, and V. Begun, Phys. Rev. C **92**, 034905 (2015).
- [48] J. R. Pelaez, arXiv:1510.00653 [hep-ph].
- [49] J. Bachler *et al.* [NA49 Collaboration], Nucl. Phys. A **661**, 45 (1999); S. V. Afanasev *et al.*, Phys. Lett. B **491**, 59 (2000); S. V. Afanasev *et al.*, J. Phys. G **27**, 367 (2001); C. Alt *et al.*, Eur. Phys. J. C **45**, 343 (2006); T. Anticic *et al.*, Eur. Phys. J. C **65**, 9 (2010); T. Anticic *et al.*, Eur. Phys. J. C **68**, 1 (2010).
- [50] G. Agakishiev *et al.* [HADES Collaboration], arXiv:1512.07070 [nucl-ex].
- [51] J. Cleymans, H. Oeschler, K. Redlich, and S. Wheaton, Phys. Rev. C **73**, 034905 (2006).
- [52] J. Stachel, A. Andronic, P. Braun-Munzinger, and K. Redlich, J. Phys. Conf. Ser. **509**, 012019 (2014).
- [53] M. Floris, Nucl. Phys. A **931**, 103 (2014).
- [54] V. Begun, EPJ Web Conf. **97**, 00003 (2015).
- [55] F. Becattini, P. Castorina, A. Milov, and H. Satz, Eur. Phys. J. C **66**, 377 (2010).
- [56] P. Castorina, D. Kharzeev, and H. Satz, Eur. Phys. J. C **52**, 187 (2007).
- [57] P. Castorina, S. Plumari, and H. Satz, arXiv:1603.06529 [hep-ph].
- [58] D. H. Rischke, M. I. Gorenstein, H. Stoecker, and W. Greiner, Z. Phys. C **51**, 485 (1991).
- [59] V. V. Begun, M. Gazdzicki, and M. I. Gorenstein, Phys. Rev. C **88**, 024902 (2013).
- [60] G. D. Yen and M. I. Gorenstein, Phys. Rev. C **59**, 2788 (1999).
- [61] V. Vovchenko and H. Stoecker, arXiv:1512.08046 [hep-ph].